Mine Water and the Environment (2021) 40:456–465
https://doi.org/10.1007/s10230-021-00780-4

TECHNICAL ARTICLE

Theoretical and Numerical Investigations of the Failure Characteristics of a Faulted Coal Mine Floor Above a Confined Aquifer

Zhengzhao Liang[1,2] · **Wencheng Song**[1,2]

Received: 17 July 2020 / Accepted: 9 April 2021 / Published online: 28 April 2021

Abstract
Mechanical models were used to analyze the failure depth of faulted and faultless mine floors based on the limit equilibrium theory of rock mass. In addition, the failure characteristics and water-inrush pathways were numerically investigated. The results were then compared, along with in-situ observations to validate these models. The mining-induced failure zone (an asymmetric "inverted saddle" shape) near the mined-out area was larger in the floor strata beneath the area around the coalface than that near the open-off cut. The maximum fault-induced failure depth was approximately twice that of the intact floor, which was generally equivalent to the in-situ observations. Three characteristic zones in the floor strata were observed during the mining process in the numerical models: a mining-induced failure area, a water-impervious area, and a fault reactivation area. The formation of the failure zone can be roughly divided into an initial stage, a stable stage, and a mutation stage. This study provides an improved understanding for predicting fault-induced mine water-inrushes.

Keywords Mining engineering · Floor failure depth · Fault zone · Theoretical model · Numerical simulation

Introduction

A serious threat associated with mining above aquifers involves uncontrolled groundwater penetrating into the workings through fractured zones in the floor strata, resulting in both economic losses and human casualties (Wang and Park 2003; Wu and Zhou 2008; Zhang 2005; Zhu and Wei 2011). Over 80% of mining incidents involving water-inrush have been linked to geological structures such as faults and karst collapse pillars (KCPs) (Bai et al. 2013; Shao et al. 2019; Zhang et al. 2014), whereas the remainder may be related to intrinsic cracks and voids within the floor srata (Lu and Wang 2015; Wang et al. 2020). In general, as shown in Fig. 1, fault zones affect the likelihood of a water in-rush, mainly by: (1) enhancing the destruction of the protective layer; (2) reducing the effective distance between the correlative aquifer and the coal body; (3) controlling the migration of groundwater. In addition, fault zones significantly increase the maximum failure depth of the floor strata compared to areas unaffected by faults, thus increasing the frequency of mining accidents (Li et al. 2011; Wu et al. 2004). Therefore, accurately determining the fault-induced failure range of post-mining strata is of crucial importance for predicting and assessing the risk of groundwater outburst in underground coal mines.

Considerable attention has been given to groundwater inrush over the past few decades, and some studies have suggested a range of empirical criteria and analytical models (Du et al. 2017; Li et al. 2018; Li and Zhou 2006; Qian et al. 2018; Zhu et al. 2014). The concept of a water-inrush coefficient was proposed and defined in the related regulation, with suggested critical values of 0.1 and 0.06 MPa m^{-1} for complex and simple structural areas, respectively (Shi et al. 2019; Sun et al. 2019a, b). Bu and Xu (2020) explained the mechanism of fault-induced groundwater inrush by adopting a simplified mechanical model to theoretically calculate the distribution of shear stress on the fault plane during coal exacavation and to systematically analyze the influence of geometrical configuration on fault reactivation. Hu et al. (2019) and Sun et al. (2019a, b) applied theoretical models associated with faults through the use of limit equilibrium theory, and successfully predicted the water-bearing

✉ Wencheng Song
dgswc@mail.dlut.edu.cn

[1] State Key Laboratory of Coastal and Offshore Engineering, Dalian University of Technology, Dalian 116024, Liaoning, China

[2] Center of Rock Instability and Seismicity Research, Dalian University of Technology, Dalian 116024, Liaoning, China

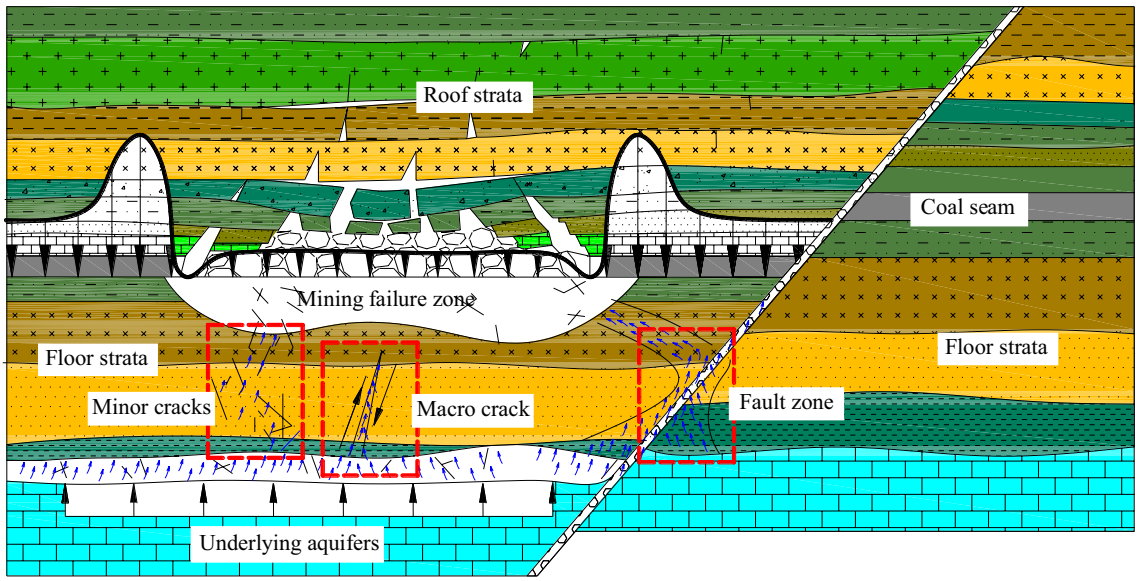

Fig. 1 Types of water inrush controlled by geologic structures

capacity of a post-mining floor. Moreover, some empirical formulas and analytical models for predicting the maximum failure zone depths were successively developed, based on hundreds of field observations (Zhai et al. 2019; Zhang and Shen 2004). Although these results have enhanced our understanding of the mechanisms and predictions of groundwater hazards, most of the approximate models or approaches reported have neglected the failure characteristics of a mine floor with faults.

Studies have adopted various approaches to better understand the hydromechanical behavior of rock mass above a confined aquifer during mining, including numerical modeling (Li et al. 2011; Yang et al. 2007), physical analogs (Zhang et al. 2017; Zhao et al. 2020; Zhu et al. 2018), and in-situ measurement (Li and Zhou 2006; Qian et al. 2018; Yin et al. 2015). Tang et al. (2002) were the first to propose the rock failure process analysis (RFPA) code for heterogeneous rock, thereby providing direct insights into the initiation, propagation and coalescence of fractures in the seam floors and the formation of inrush channels around the faults. Wu et al. (2004) proposed that groundwater bursting along the fault zone could either be instantaneous or delayed after the formation of a roadway or mined-out area. Zhang et al. (2017) used a laboratory experiment to observe the entire water inrush process, thereby identifying the hydrological connection between the failure zone and the underlying aquifer, facilitated by the fault reactivation zone as the cause of the formation of an inrush pathway. Lu and Wang (2013) and Sun and Wang (2013) used micro-seismic monitoring to determine that the failure depths of faulted mine floors are about twice those of mine faultless floors, thereby dramatically increasing the risk of water inrush. Although previous studies have contributed greatly to evaluating the risk of water inrush, there remains a lack of knowledge, particularly with regard to appropriate theoretical models.

To this end, the current study developed analytical models based on the limit equilibrium theory of rock mass to predict the maximum failure depth of faulted and faultless floors after mining. Also, the influence of mining on the fault-induced failure range and inrush pathway of the floor was numerically investigated using fast Lagrangian analysis of continua (FLAC3D).

Geology

The Huatai coal mine is located within Laiwu city, Shandong Province, in northern China. This mine has a field area of ≈ 27.3 km^2; the nos. 2, 4, 7, and 15 seams are minable. The geological data indicate that working face 7502, mining the No. 7 seam, is roughly horizontal, with an average thickness of 4 m, a mining depth of 650 m, and a mining width of 150 m. The normal fault F_{qin}, which affects the excavation process of working face 7502, falls within the main structure in the middle of the coalfield. Moreover, as shown in Fig. 2, a limestone aquifer with a measured hydraulic pressure exceeding 3.2 MPa lies 63 m directly beneath the coal seam. Past evidence has demonstrated the need to evaluate and predict the risk of a groundwater outburst near the faulted area, where the water in-rush coefficient is close to the critical value of 0.06 MP m^{-1}.

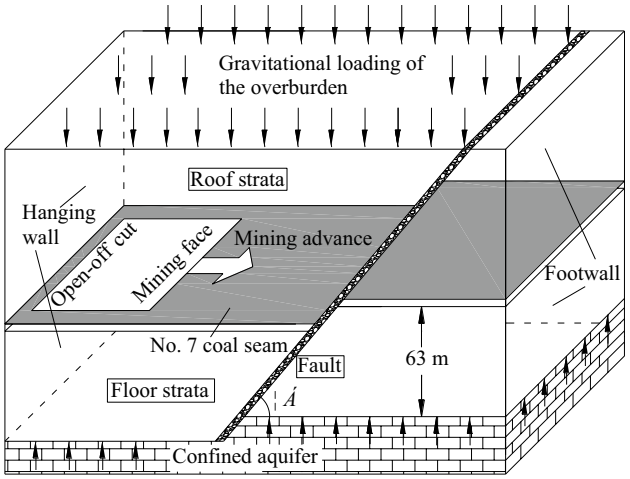

Fig. 2 Engineering geological model of working face No. 7502 in the Huatai Coal Mine

Theoretical Analysis

Model Construction

The excavation of mines above an underlying aquifer, and especially above the Ordovician limestone aquifer, will lead to a redistribution of geo-stress and strata failure around these excavations (Yin et al. 2015), with a possibility of the floor stratum being subjected to both excavation-induced and groundwater pressures. Li et al. (2011) found a correlation between coal seam excavation and floor deformation, with three significant areas of deterioration: the "mining-disturbed area", the "water-impervious area" and the "aquifer ascending area". Figure 3 shows the mechanical models for faulted and faultless floors, where x indicates the mining direction along the working face with a length of L, and z denotes the downward direction perpendicular to the coal seam floor with a height of H_z. The model represents the load of rock mass induced by roof caving as an equivalent uniformly distributed load with a value of γH_m. Groundwater pressure in the underlying confined aquifer increases the risk of the floor strata expanding into the exposed space of the excavated area during the mining process. Consequently, the risk of water inrush increases with increasing hydraulic pressure.

Model Derivation

This paper provides the detailed derivation of only the fault-related model due to space limitations. A micro-element with a thickness of dz can be extracted from the water-impervious layer, with the associated element stress analysis shown in Fig. 3a. Based on the limit equilibrium theory of rock mass,

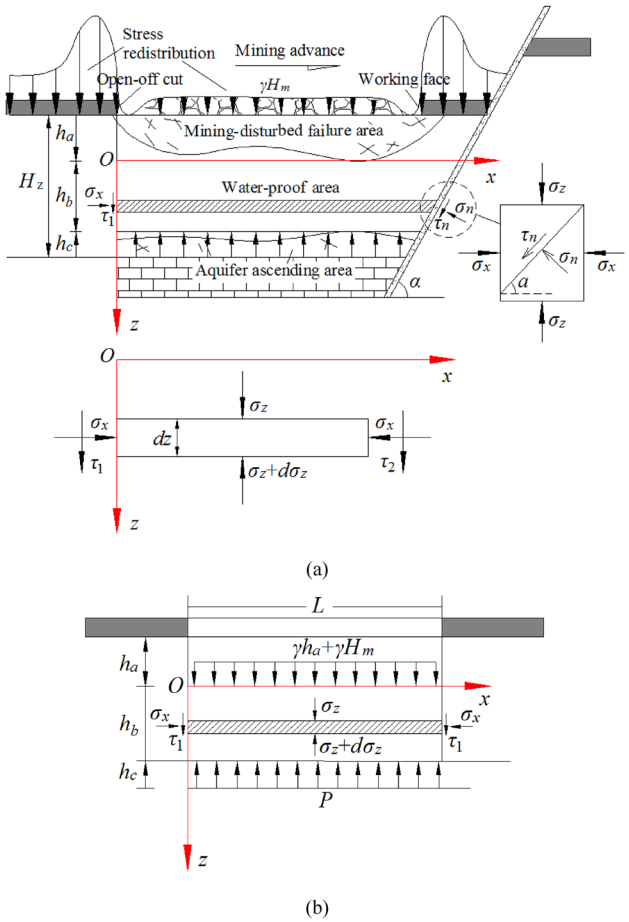

Fig. 3 Mechanical models and element stress analysis based on the limit equilibrium theory of rock mass. **a** faulted floor; **b** faultless floor

Eq. (1) should be satisfied to maintain the mechanical equilibrium of the element body along the z direction.

$$(\sigma_z + d\sigma_z - \sigma_z)L - (\tau_1 + \tau_2)dz = 0 \tag{1}$$

According to the Mohr–Coulomb criterion (Shen and Chen 2006), the friction resistances τ_1 and τ_2 on both sides of the unit body are given in Eq. (2).

$$\left.\begin{aligned} \tau_1 &= C + \sigma_x \tan\varphi \\ \tau_2 &= \left(C_f + \sigma_x \tan\varphi_f\right)\sin\alpha \end{aligned}\right\} \tag{2}$$

where C and C_f denote the cohesion of the floor strata and the fault zone respectively, φ and φ_f refer to the corresponding internal friction angle, and α indicates fault dip.

Equation (3) can then be obtained by substituting Eq. (2) into Eq. (1):

$$\frac{d\sigma_z}{dz} = \frac{\tan\varphi + \tan\varphi_f \sin\alpha}{L}\sigma_x + \frac{C + C_f \sin\alpha}{L} \tag{3}$$

Given that Eq. (4) is satisfied, then the yielding failure of rock begins to occur under limit equilibrium conditions (Sun et al. 2019a, b).

$$\frac{\sigma_z + C\cot\varphi}{\sigma_x + C\cot\varphi} = \frac{1+\sin\varphi}{1-\sin\varphi} \tag{4}$$

Assuming that $\frac{1+\sin\varphi}{1-\sin\varphi} = \lambda$, Eq. (5) can be obtained by solving Eq. (3) and Eq. (4):

$$\sigma_z = Ae^{\frac{(\tan\varphi+\tan\varphi_f\sin\alpha)}{\lambda L}z} - \frac{C+\lambda C_f\sin\alpha+\tan\varphi_f\cot\varphi(1-\lambda)C\sin\alpha}{\tan\varphi+\tan\varphi_f\sin\alpha} \tag{5}$$

In Eq. (5), A denotes the undetermined coefficient. Considering the effect of roof caving on the coal seam floor, the boundary conditions of the model derived in Fig. 3a are:

$$\left.\begin{array}{l} z=0,\ \sigma_z = rh_a + rH_m \\ z=H_z-h_a-h_c,\ \sigma_z = P - r\left(H_z-h_c\right) - rH_m \end{array}\right\} \tag{6}$$

Accordingly, the maximum failure depth (h_a) of a faulted floor after mining can be expressed implicitly, as shown in Eq. (7):

$$h_a = \frac{P - \left[\gamma H_m + \frac{C+\lambda C_f\sin\alpha+\tan\varphi_f\cot\varphi(1-\lambda)C\sin\alpha}{\tan\varphi+\tan\varphi_f\sin\alpha}\right]e^{\frac{(\tan\varphi+\tan\varphi_f\sin\alpha)(H_z-h_a-h_c)}{\lambda L}} + \frac{C+\lambda C_f\sin\alpha+\tan\varphi_f\cot\varphi(1-\lambda)C\sin\alpha}{\tan\varphi+\tan\varphi_f\sin\alpha} - \left[\gamma\left(H_z-h_a-h_c\right)+\gamma H_m\right]}{\gamma\left[1+e^{\frac{(\tan\varphi+\tan\varphi_f\sin\alpha)(H_z-h_a-h_c)}{\lambda L}}\right]} \tag{7}$$

where h_a and h_c denote the mining-disturbed failure depth and the hydraulic ascending height, respectively, P is the hydraulic pressure in the underlying aquifer, γ represents the average bulk density of the rock stratum, L represents the mining distance of the coalface, H_z is the distance between the coal seam and the correlative aquifer, H_m indicates the caving height of roof strata induced by coal extraction, and the remaining parameters are the same as those defined previously. As shown in Eq. (8), H_m can be defined according to Liang et al. (2020) and Zhang and Shen (2004).

$$H_m = \frac{100\sum M}{1.6\sum M + 3.6} \pm 5.6 \tag{8}$$

In Eq. (8), ΣM denotes the cumulative mining thickness of the coal seam. Similarly, the excavation-induced damage depth of a faultless floor, as evident in Fig. 3b, is derived as follows:

$$h_a = \frac{P - \left[\gamma H_m + C\cot\varphi\right]e^{\frac{2\tan\varphi(H_z-h_a-h_c)}{\lambda L}} + C\cot\varphi - \left[\gamma\left(H_z-h_a-h_c\right)+\gamma H_m\right]}{\gamma\left[1+e^{\frac{2\tan\varphi(H_z-h_a-h_c)}{\lambda L}}\right]} \tag{9}$$

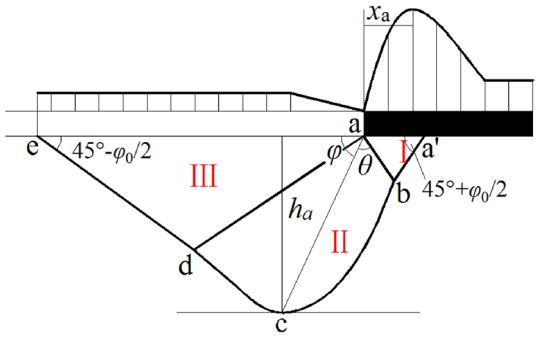

Fig. 4 Traditional slipping line mechanical model presented by Zhang

Therefore, Eq. (7) and Eq. (9) can be used to analyze and predict the range of the mining-disturbed area in faulted and faultless floors, respectively.

Failure Depth Calculation

During the mining process, the floor strata will inevitably be subjected to mechanical loads, which gradually cause the expansion of pre-existing cracks (or weakness), thus forming failure zones around the excavations. The mining-disturbed failure zone in the fault-free floor (Fig. 4), has conventionally been represented as having three different regions: (1) the active area; (2) the transition area; and (3) the passive area.

According to Zhang (2005), the maximum depth of the fracture in its most general form, which depends on the yield length of the coal pillar positioned around the coalface and the friction angle of the floor strata, is derived by:

$$h_a = \frac{x_a\cos\varphi_0}{2\cos\left(\frac{\pi}{4}+\frac{\varphi_0}{2}\right)}e^{\left(\frac{\pi}{4}+\frac{\varphi_0}{2}\right)\tan\varphi_0} \tag{10}$$

where x_a is the yield length of the coal pillar, with an empirical value of $x_a = 0.015H$ (H denotes the average mining depth of the coal seam) and φ_0 denotes the internal friction angle of the floor strata. The mining and geological records of the Huatai coal mine were used to suggest the

configuration parameters of the models shown in Figs. 3 and 4: $H=650$ m,φ (φ_0)$=33°$, $\varphi_f=28°$, $\gamma=25$ kN m^{-3}, $M=4$ m, $\alpha=30°$, 45° and 60°, $H_z=63$ m, $h_c=8$ m, $L=160$ m, $C=5$ MPa, $C_f=0.7$ MPa, and $P=4$ MPa. The failure depths in the faulted and faultless floors disturbed by mining can be obtained by substituting these parameters into Eq. 7, 9, and 10, respectively (Table 1).

The maximum damaged depth of a floor without faults can reach up to 15.63 m after mining, which is roughly consistent with the 17.14 m calculated using the slip-line mechanical theory. In contrast, the maximum excavation-induced failure depth of the floor with varying fault dips ranges from 31.08 to 35.34 m. Thus, the damaged depth of a faulted floor exceeds that of a faultless floor by a factor of 1.81–2.26.

Numerical Simulation

In general, many factors affect water-inrush from a faulted mine floor. While geological structures, such as faults, are the main factors controlling water inrush, mining pressure tends to induce water inrush by creating a hydraulic link between the floor strata and the underlying aquifer. In addition, the aquifer's water abundance, manifested as hydraulic pressure, is the driving force determining the occurrence of a groundwater outburst. We used FLAC^{3D} software (Itasca Consulting Group, Inc. 2005, version 3.0) to obtain more detailed observations of the failure characteristics and inrush pathway of a faulted floor during the mining process above a confined aquifer.

Model Settings and Scenarios

According to the primary geological and geometric conditions of the Huafeng coal mine, Fig. 5 shows three case studies with fault dips of 30°, 45°, and 60°, which are mainly composed of five equivalent layers: roof strata, the coal seam, floor strata, the fault zone, and the confined aquifer. These models were discretized into a mesh of X, Y, and Z dimensions of 360 m × 230 m × 150 m, involving a total of 37,214 elements. A stepwise excavation method was adopted in the numerical calculation to clearly demonstrate the mining process, with each step advancing 10 m forward from X = 40 m until water inrush occurred. Simultaneously, all of the models were analyzed by hydro-mechanical coupling to characterize the damage and flow in the seam floors during coal mining.

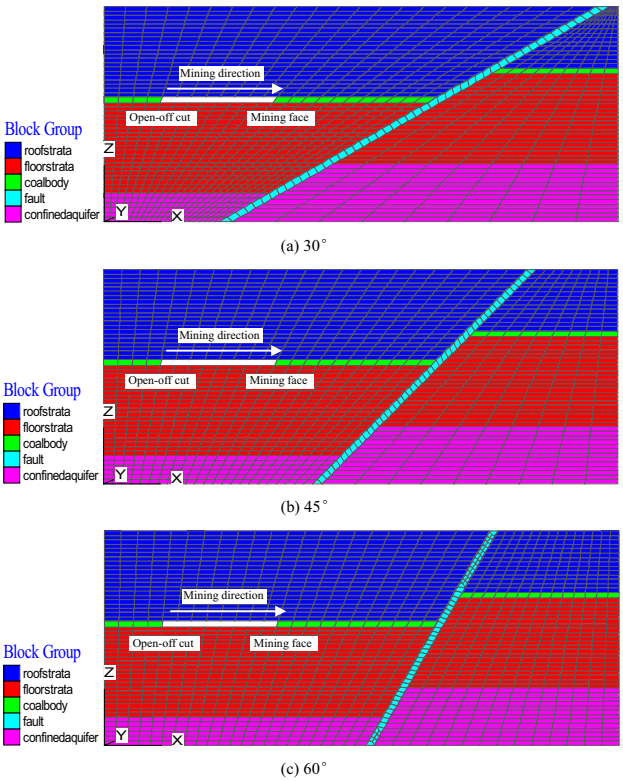

Fig. 5 Numerical models for coal seam mining with a faulted floor

An equivalent load of $\sigma_z=14.67$ MPa was applied uniformly on the upper boundary to simulate geo-stress caused by overburden layers, with a depth of about 600 m. The lower boundary of the model was fully constrained, and the hydraulic pressure in the aquifer was set at 4 MPa. The rest of the model's boundaries were horizontally constrained. As shown in Table 2, the physico-mechanical

Table 1 The theoretically obtained results of maximum failure depth of the No. 7502 working face

Floor property	Fault dip/(°)	Mining-induced failure depth/(m)		Ratio /(Faulted/Faultless)
		Limit equilibrium theory	Slip-line theory	
Faulted floor	30°	31.08	*	1.81–2.26 2.04
	45°	33.69	*	
	60°	35.34	*	
Faultless floor	*	15.63	17.14	

*indicates that such case does not exist in the calculation scheme

Table 2 Physico-mechanical parameters for rocks and the coal seam employed in the numerical simulation

Lithology	Density/ (kN m^{-3})	Bulk modulus/GPa	Shear modulus/GPa	Cohesion/MPa	Friction angle /(°)	Tensile strength/MPa	Permeability/ (m^2·(Pa·sec)$^{-1}$)	Porosity
Roof strata	25.0	5.0	3.2	4.0	32	3.0	6×10^{-15}	0.3
Coal seam	13.9	2.3	2.0	2.1	20	1.1	3×10^{-13}	0.4
Floor strata	25.0	6.0	4.1	5.0	33	2.8	7×10^{-15}	0.2
Fault zone	21.0	1.0	1.25	0.7	28	0.2	5×10^{-12}	0.5
Confined aquifer	24.0	4.0	2.3	2.0	31	2.1	4×10^{-10}	0.7

parameters of rocks and the coal seam in the simulations were empirically chosen and estimated according to the results of field testing.

Numerical Results and Analysis

The current study numerically analyzed the influence of faults on the floor failure range after mining. As evident in Fig. 6, the configurations of the failure zones around the open-off cut and the mining face were asymmetric in the mined-out area, with the latter distributed over a larger range than the former. This was markedly different from the symmetrical "inverted saddle" failure pattern of a faultless floor (Li 1999; Song et al. 2019). Additionally, the simulated results showed that there is a possibility of the confined water (indicated in red in Fig. 6, showing the flow vectors rising along the fault) bursting into the mined-out area through the damaged zone below or in

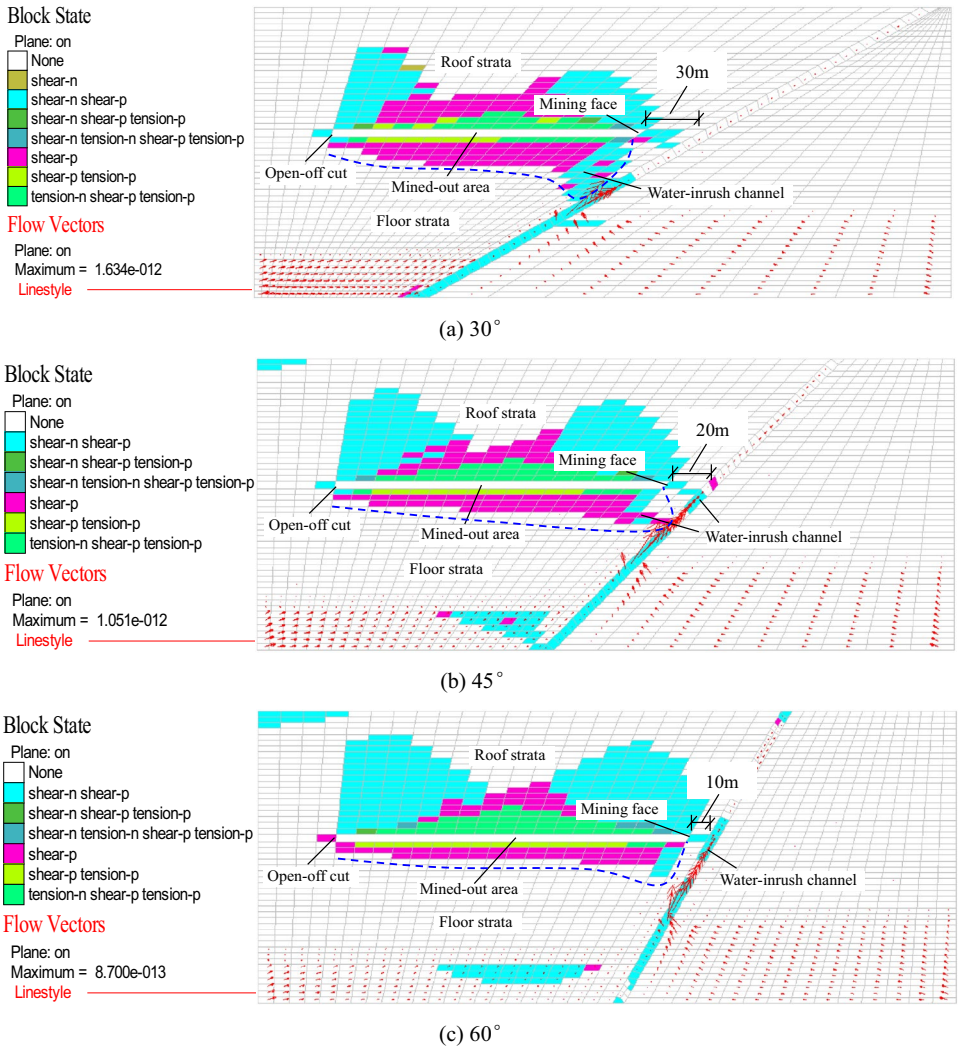

Fig. 6 Profiles of failure state in the seam floors during the formation of a water-inrush pathway

front of the working face. This may provide a theoretical basis for the previous study on fracture zones as the main pathway of water-inrush (Biswas and Sharma 2017).

Within the practice of coal mining above aquifers, the quantitative and comparative determination of the floor failure range is vitally important to further evaluate water-inrush risk in underground coal mines. Figure 7 shows the relationships between the mining-induced failure depth, the fault-activated height, and the mining distance. It should be noted that all models presented a similar floor failure process trend with varying fault dips being roughly divided into three stages: (A) initial; (B) stable,

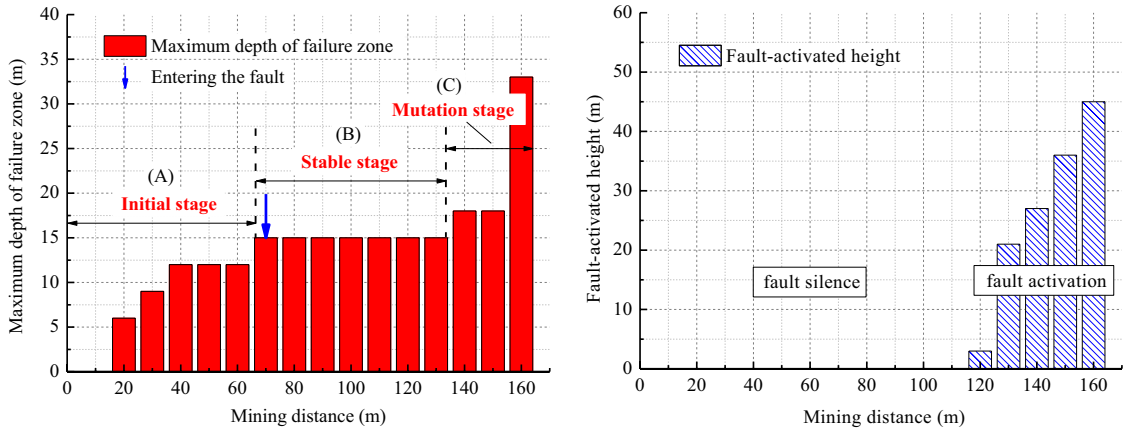

(a) 30°

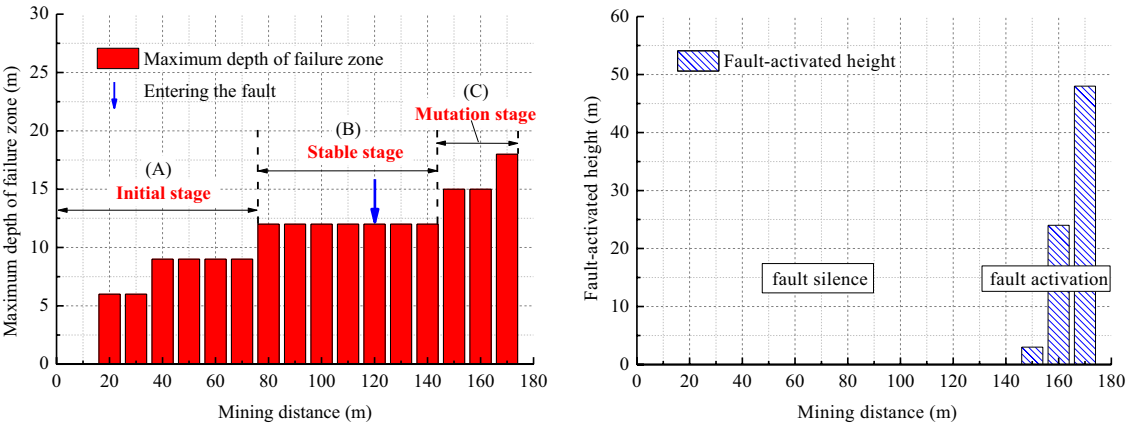

(b) 45°

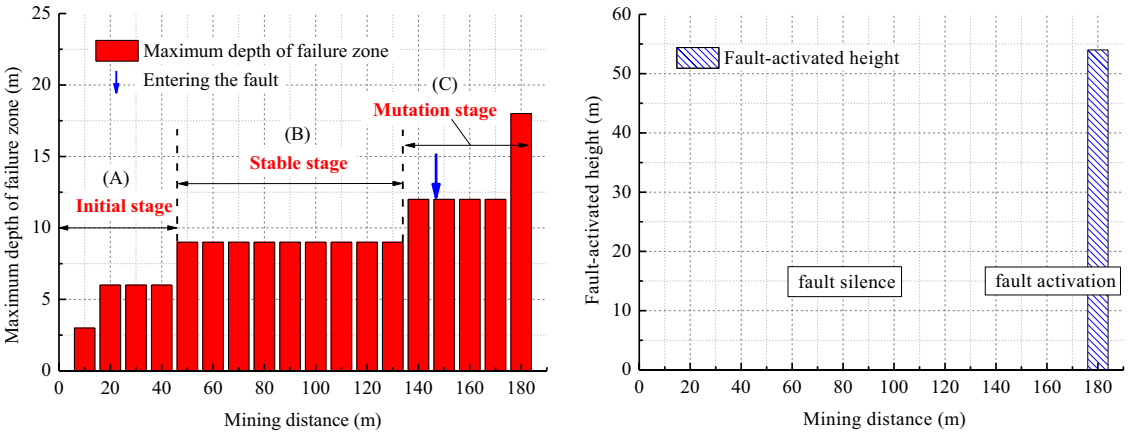

(c) 60°

Fig. 7 Relationships between the mining-induced failure depth, the fault-activated height and the mining distance

and (C) mutation. Moreover, the activation processes of faults with dip angles of 30°, 45°, and 60° mainly fell in the mutation stage.

As shown in Figs. 7a and 8, under an inclination angle $\alpha = 30°$, the failure depth of the floor during the initial stage (0–60 m) gradually increased as the coal seam was excavated. The failure depth remained basically unchanged during the stable stage (60–130 m) (Fig. 8b), whereas the failure depth continually extended forward in the failure range (volume) as the mining face advanced. The failure boundary approximates a straight line parallel to the coal seam floor. However, with further excavation (130–160 m, i.e., the mutation stage), the failure zone propagated downwards in an asymmetric manner, where the right part of the damaged floor was clearly wider and deeper than that of the left side (Fig. 8c). Meanwhile, there was a potential for further activation of the fault, with the reactivated fault being more active, with newly damage continuously appearing around the fault. The damage developed gradually, with fractures connecting to form a highly permeable pathway between the damaged zone in the floor strata and the fault, as the advancing distance approached a critical value of 160 m (Fig. 8d).

In addition, three characteristic zones were routinely observed in the mining floor in the vertical direction: (1) a mining-induced failure zone; (2) an intact (or water-impervious) zone; and (3) a fault reactivation zone. Once the scattered fractures in the fault reactivation zone were hydraulically connected with the mining-induced failure zone, large volumes of groundwater could enter the workings in an uncontrollable manner, thereby resulting in water inrush.

This maximum failure depth appeared in the floor strata beneath the area around the coal wall, whereas that of the faultless floor could be roughly determined before the working face entered the horizontal projection of the fault onto the coal floor. Table 3 shows the results of the numerical analysis.

These results demonstrate significant differences in the failure depth and morphology of the post-mining floor due to the influence of faults. The maximum damage depth of the mine floor related to faults was about twice that of the intact floor. This result is consistent with micro-seismic monitoring reported by Lu and Wang (2013) and Sun and Wang (2013). Table 4 lists the typical results of floor failure depth measured in different coal mines. Qualitatively, the phenomena

Table 3 The numerically simulated results of floor failure depth of the No. 7502 working face

Fault dip/(°)	Mining-induced failure depth/(m)		Ratio/(Faulted/Faultless)	Average ratio/(Faulted/Faultless)
	Faulted floor	Faultless floor (before entering the fault)		
30°	33	12	2.75	2.08
45°	18	12	1.50	
60°	18	9	2.00	

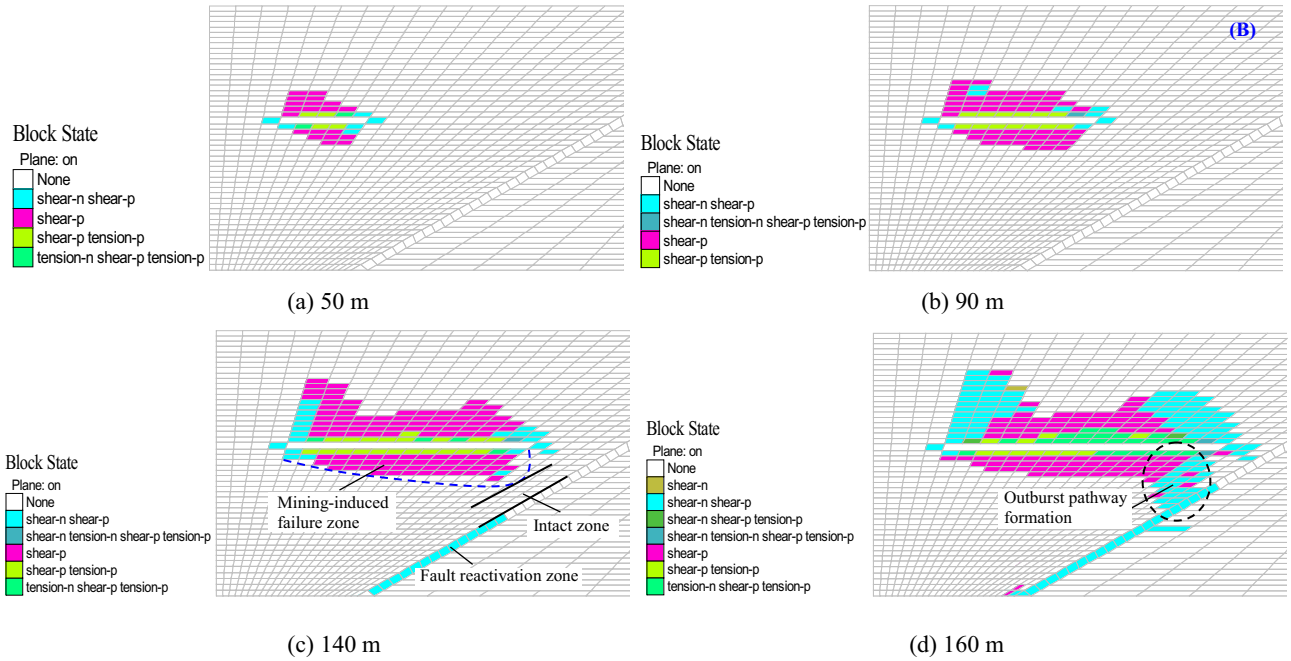

Fig. 8 Profiles of the change in damage in the seam floor with varying mined distances. (a case with inclination angle $\alpha = 30°$)

Table 4 Typical results of floor failure depth measured in different coal mines

No	Working face and its location	Mining geological conditions				Measured failure depth/(m)	Ratio/(h_1/h_0)
		Mining depth/(m)	Mining thickness/(m)	Face width/(m)	Fault property		
1	No. 2701-1 working face (Fengfeng No.2 Coal Mine)	145	1.5	120	0	14.0	1.29
	No. 2701-2 working face (Fengfeng No.2 Coal Mine)	145	1.5	120	1	18.0	
2	No. 5701-1 working face (Jingjing No.3 Coal Mine)	227	3.5	30	0	3.5	2.00
	No. 5701-2 working face (Jingjing No.3 Coal Mine)	227	3.5	30	1	7.0	
3	No. 4303-1 working face (Xinzhuangzi Coal Mine)	310	1.8	128	0	16.8	1.76
	No. 4303-2 working face (Xinzhuangzi Coal Mine)	310	1.8	128	1	29.6	
4	No. 1066 working face (Taoyuan Coal Mine)	490	3.4	112	1	16.2 (0), 30.4 (1)	1.87

encountered follow this trend, which is also generally consistent with theoretical and numerical observations. Results from such analyses could provide a theoretical explanation for the frequent occurrence of groundwater inrush accidents in some coal mines when the working face is adjacent to the fault during the mining process (Wu et al. 2004; Zhang et al. 1997).

Conclusions and Discussion

The current study employed both theoretical and numerical models along with in-situ observations to comparatively investigate the failure characteristics of faulted and faultless floors after mining. The main results can be summarized as follows:

(1) The current study derived mechanical models considering the roof caving load and the hydraulic pressure in the aquifer, which were used to calculate the theoretical failure depths of faulted and faultless floors. The theoretically and numerically obtained results showed that the maximum damaged depth of a faulted mine floor was about twice that of the intact floor, similar to in-situ observations. After the formation of an inrush pathway, the failure zone around presented an asymmetric "inverted saddle" shape near the mined-out area, which was obviously wider and deeper near the coalface than near the open-off cut. In other words, the maximum failure depth appeared in the floor strata beneath the area around the coal wall of the working face.

(2) The failure process of floors with fault dips of 30°, 45°, and 60° could be roughly divided into three stages during the mining processes: (1) initial; (2) stable, and (3) mutation. In addition, the activation processes of faults with varying dips mainly fell in the mutation stage. This indicates that measures such as goaf filling or floor grouting should be used to improve the mining safety of underground coal mines.

(3) The numerical observations showed that the floor strata in the vertical direction could be classified into three distinct damaged zones: (1) a mining-induced failure zone; (2) an intact zone, and (3) a fault reactivation zone. The confined water was prone to rise along the fault reactivation zone and penetrate into the mined-out area through the fracture zone below or in front of the working face. Therefore, a water-impervious pillar with a critical length of 30 m should be preserved to effectively prevent inrush hazards.

(4) The analytical models developed in the present study are beneficial to a comparative analysis between the failure depths of faulted and faultless floors. Although the current study shows limitations in representing the fracturing process of floor rock mass in underground geo-engineering, the presented models do reveal the underlying theoretical mechanism resulting in the frequent occurrence of inrush disasters in some coal mines when the working face is adjacent to the fault, thus providing a basis for the assessment and treatment of water inrushes from underlying aquifers.

Acknowledgements Mr. Wang Jianning provided great assistance with in-situ observations and data processing and Mrs. Wu Na provided

constructive suggestions on the paper's framework. This study was supported by the National Natural Science Foundation of China (41977219, 51779031) and the Open Fund of State Key Laboratory of Coal Resources and Safe Mining (Grant SKLCRSMI9KFA02).

References

Bai HB, Ma D, Chen ZQ (2013) Mechanical behavior of groundwater seepage in karst collapse pillars. Eng Geol 164:101–106

Biswas A, Sharma SP (2017) Geophysical surveys for identifying source and pathways of subsurface water inflow at the Bangur chromite mine, Odisha, India. Nat Hazards 88(2):947–964

Bu WK, Xu H (2020) Research on the effect of dip angle on shear stress on normal fault plane and water inrush in floor strata during mining activities. Geotech Geol Eng 38(5):4407–4421

Du WS, Jiang YD, Ma ZQ, Jiao ZH (2017) Assessment of water inrush and factor sensitivity analysis in an amalgamated coal mine in China. Arab J Geosci 10(21):471

Hu Y, Sun J, Liu WQ, Wei DY (2019) The evolution and prevention of water inrush due to fault activation at working face no. ii 632 in the Hengyuan coal mine. Mine Water Environ 38(1):93–103

Itasca Consulting Group, Inc. (2005) Fast Lagrangian analysis of continua in 3 dimensions, version 3.0, user's manual. Itasca Consulting Group, Inc.

Li BY (1999) "Down three zones" in the prediction of water inrush from coalbed floor aquifer: theory, development and application. J Shandong Inst Min Tech 18(4):11–18 (**in Chinese**)

Li GY, Zhou W (2006) Impact of karst water on coal mining in north China. Environ Geol 49(3):449–457

Li LC, Yang TH, Liang ZZ, Zhu WC, Tang CA (2011) Numerical investigation of groundwater outbursts near faults in underground coal mines. Int J Coal Geol 85(3–4):276–288

Li WP, Liu Y, Qiao W, Zhao CX, Yang DD, Guo QC (2018) An improved vulnerability assessment model for floor water bursting from a confined aquifer based on the water inrush coefficient method. Mine Water Environ 37(1):196–204

Liang ZZ, Song WC, Liu WT (2020) Theoretical models for simulating the failure range and stability of inclined floor strata induced by mining and hydraulic pressure. Int J Rock Mech Min Sci 132:104382

Lu YL, Wang LG (2013) Modeling and microseismic monitoring of damage and failure evolution of faulty coal seam floor. J Min Safety Eng 30(1):38–44 (**in Chinese**)

Lu YL, Wang LG (2015) Numerical simulation of mining-induced fracture evolution and water flow in coal seam floor above a confined aquifer. Comput Geotech 67:157–171

Qian ZW, Huang Z, Song JG (2018) A case study of water inrush incident through fault zone in China and the corresponding treatment measures. Arab J Geosci 11(14):381

Shao JL, Zhou F, Sun WB (2019) Evolution model of seepage characteristics in the process of water inrush in faults. Geofluids 10:1–14

Shen MR, Chen JF (2006) Mechanics of rock masses. Tongji University Publishing House, Shanghai (in Chinese)

Shi LQ, Qiu M, Wang Y, Qu XY, Liu TH (2019) Evaluation of water inrush from underlying aquifers by using a modified water-inrush coefficient model and water-inrush index model: a case study in Feicheng coalfield, China. Hydrogeol J 27(6):2105–2119

Song WC, Liang ZZ, Liu WT, Zhao CB (2019) Theoretical analysis and experimental investigation on failure characteristics and stability of stope floor. Chin J Rock Mech Eng 38(11):2208–2218 (**in Chinese**)

Sun J, Wang LG (2013) Floor fault water-inrush prediction based on catastrophe analysis of micro-seismic signals. J China Coal Society 38(8):102–108 (**in Chinese**)

Sun J, Wang LG, Hu Y (2019a) Mechanical criteria and sensitivity analysis of water inrush through a mining fault above confined aquifers. Arab J Geosci 12(1):4

Sun WB, Xue YC, Li TT, Liu WW (2019b) Multi-field coupling of water inrush channel formation in a deep mine with a buried fault. Mine Water Environ 38(3):528–535

Tang CA, Tham LG, Lee PKK, Yang TH, Li LC (2002) Coupled analysis of flow, stress and damage (FSD) in rock failure. Int J Rock Mech Min Sci 39(4):477–489

Wang JA, Park HD (2003) Coal mining above a confined aquifer. Int J Rock Mech Min Sci 40(4):537–551

Wang X, Yuan W, Yan YT, Zhang X (2020) Scale effect of mechanical properties of jointed rock mass: a numerical study based on particle flow code. Geomech Eng 21(3):259–268

Wu Q, Zhou WF (2008) Prediction of groundwater inrush into coal mines from aquifers underlying the coal seams in China: vulnerability index method and its construction. Environ Geol Water Sci 56(2):245–254

Wu Q, Wang M, Wu X (2004) Investigations of groundwater bursting into coal mine seam floors from fault zones. Int J Rock Mech Min Sci 41(4):557–571

Yang TH, Liu J, Zhu WC, Elsworth D, Tham LG, Tang CA (2007) A coupled flow-stress-damage model for groundwater outbursts from an underlying aquifer into mining excavations. Int J Rock Mech Min Sci 44(1):87–97

Yin S, Zhang J, Liu D (2015) A study of mine water inrushes by measurements of in situ stress and rock failures. Nat Hazards 79(3):1961–1979

Zhai JH, Liu DL, Li G, Wang FT (2019) Floor failure evolution mechanism for a fully mechanized longwall mining face above a confined aquifer. Adv Civ Eng 2019:1–11

Zhang JC (2005) Investigations of water inrushes from aquifers under coal seams. Int J Rock Mech Min Sci 42(3):350–360

Zhang JC, Shen BH (2004) Coal mining under aquifers in china: a case study. Int J Rock Mech Min Sci 41(4):629–639

Zhang JC, Zhang YZ, Liu TQ (1997) Seepage of rock mass and water inrush from coal seam floor. Geological Publishing House, Beijing (**in Chinese**)

Zhang R, Jiang ZQ, Zhou HY, Yang CW, Xiao SJ (2014) Groundwater outbursts from faults above a confined aquifer in the coal mining. Nat Hazards 71(3):1861–1872

Zhang SC, Guo WJ, Li YY, Sun WB, Yin DW (2017) Experimental simulation of fault water inrush channel evolution in a coal mine floor. Mine Water Environ 36(3):443–451

Zhao JH, Zhang XG, Jiang N, Yin LM, Guo WJ (2020) Porosity zoning characteristics of fault floor under fluid-solid coupling. B Eng Geol Environ 79(5):2529–2541

Zhu WC, Wei CH (2011) Numerical simulation on mining-induced water inrushes related to geologic structures using a damage-based hydromechanical model. Environ Earth Sci 62(1):43–54

Zhu B, Wu Q, Yang JW, Cui T (2014) Study of pore pressure change during mining and its application on water inrush prevention: a numerical simulation case in Zhaogezhuang coalmine, China. Environ Earth Sci 71(5):2115–2132

Zhu GL, Zhang WQ, Wang SL, Zhang PS (2018) Experimental research on characteristics of fault activation and confined water rising. Geotech Geol Eng 36(4):2625–2636